



Cryogenic Solid Solubility Measurements for HFC-32 + CO₂ Binary Mixtures at Temperatures Between (132 and 217) K

Mirhadi S. Sadaghiani¹ · Arman Siahvashi¹ · Arash Arami-Niya^{1,2} · Tomoya Tsuji³ · Atsuhiko Yukumoto⁴ · Yoshio Seiki⁴ · Saif Z. S. Al Ghafri¹ · Paul L. Stanwix¹ · Eric F. May^{1,5}

Received: 2 May 2023 / Accepted: 17 July 2023 / Published online: 11 August 2023
© The Author(s) 2023

Abstract

Accurate phase equilibrium data for mixtures of eco-friendly but mildly-flammable refrigerants with inert components like CO₂ will help the refrigeration industry safely employ working fluids with 80 % less global warming potential than those of many widely-used refrigerants. In this work, a visual high-pressure measurement setup was used to measure solid–fluid equilibrium (SFE) of HFC-32 + CO₂ binary systems at temperatures between (132 and 217) K. The experimental data show a eutectic composition of around 11 mol % CO₂ with a eutectic temperature of 131.9 K at solid–liquid–vapour (SLVE) condition. Measured SLVE and solid–liquid equilibrium data were used to tune a thermodynamic model implemented in the ThermoFAST software package by adjusting the binary interaction parameter (BIP) in the Peng–Robinson equation of state. The tuned model represents the measured melting points for binary mixtures with a root mean square deviation (RMSD) of 3.2 K, which is 60 % less than achieved with the default BIP. An RMSD of 0.5 K was obtained using the tuned model for the mixtures with CO₂ fractions over 28 mol % relative to an RMSD of 3.4 K obtained with the default model. The new property data and improved model presented in this work will help avoid solid deposition risk in cryogenic applications of the HFC-32 + CO₂ binary system and promote wider applications of more environmentally-friendly refrigerant mixtures.

Keywords Carbon dioxide · Freeze-out risk · Global warming potential · HFC-32 · Refrigeration · Thermodynamic model

1 Introduction

The hydrofluorocarbons (HFCs) of HFC-32, HFC-134a and HFC-125 are refrigerants commonly used as working fluids in domestic air-conditioning systems, with global warming potentials (GWPs) of 677, 1300 and 3170 over a 100-year time scale, respectively [1]. Of the three HFCs, HFC-32 has the lowest atmospheric lifetime of 5.2 years (80 % less than the other HFCs) and better heat transfer properties [1]. However, its moderate flammability and toxic combustion products pose safety hazards to public users and are barriers to its widespread replacement [2]. Therefore, HFC-32 is often blended with non-flammable HFC-125 in binary mixtures of HFC-410A (HFC-32/HFC-125: 50/50 wt %) and HFC-410B (HFC-32/HFC-125: 45/55 wt %) to neutralise its flammability and ensure safe use in domestic refrigeration systems [3]. These blends, however, have GWPs of 2235 (HFC-410A) and 2328 (HFC-410B), which do not satisfy the refrigerant regulation objectives of the Montreal Protocol and the Kigali Amendment [4].

Carbon dioxide (CO_2), as a natural refrigerant, can be blended with HFC-32 to neutralise its flammability and significantly reduce the overall GWP of the mixture with minor reductions in HFC-32's cooling performance. To efficiently use the HFC-32 + CO_2 binary system as the working fluid in refrigeration systems, reliable predictions of its thermophysical properties across a wide range of working temperatures and pressures are necessary. The thermophysical properties of this binary mixture have been well studied at relatively high operating temperatures, as shown in Table 1. However, because CO_2 has a triple point of 216.55 K at 0.518 MPa [5] the risk of freeze-out at lower operating temperatures can be significant, with solid crystals potentially damaging equipment or blocking flow [6]. Therefore, solid formation at low temperatures needs to be investigated. Although some solid–fluid equilibrium (SFE) data for HFC-32 + CO_2 binary mixtures have been reported at the three-phase equilibrium line of the binary mixture [7], no experimental SFE data have been reported at elevated pressures for this system.

The study and improved prediction of fluid mixture properties, particularly those containing CO_2 , as well as the description of SFE, builds upon the many significant contributions made by Prof Roland Span to the field of thermodynamics. These include

Table 1 Summary of the thermodynamic property data available for HFC-32 + CO_2 binary mixtures

Properties	Range (T, p, z) ^a	References
$p\nu T_x$	303 to 343 K, 0.14 to 4.6 MPa, 0.17 to 0.8	[8]
VLE	289 to 290 K, 1.4 to 3.6 MPa, 0.04 to 0.8	[9]
VLE	280 to 310 K, 1.7 to 6.4 MPa, 0.21 to 0.8	[10]
VLE	222 to 283 K, 0.1 to 4.5 MPa, 0 to 1.0	[11]
VLE	283 to 343 K, 1.1 to 6.6 MPa, 0 to 1.0	[12]
VLE	293 K, 1.8 to 4.8 MPa, 0.09 to 0.89	[13]
VLE	223 to 273 K, 0.3 to 2.7 MPa, 0.1 to 1.0	[14]
SLVE	137 to 217 K, 0.03 to 0.5 MPa, 0 to 1.0	[7]

^a z represents the mole fraction of CO_2 in the binary mixtures

the development of reference equations of state (EOS) for pure fluids [5] and fluid mixtures [15], as well as the development of fundamental EOS that better describe solid phase properties, including their equilibria with fluid mixtures [16–18]. In this work, the SFE of HFC-32+CO₂ binary mixtures was measured at CO₂ concentrations between (0 and 100) mol % and pressures up to 11 MPa using a synthetic method described previously [19–21]. The measured data were then compared with the predictions of a thermodynamic model consisting of a Peng–Robinson 1976 EOS for the fluid phase [22] and a reference EOS for the CO₂ solid phase (I) [23] implemented in the ThermoFAST software package [24]. The EOS describing the fluid mixture was then tuned to the experimental SFE data.

2 Experimental

2.1 Apparatus Overview

The measurement setup, shown in Fig. 1a, b and described previously [19, 25–27], was used for SFE determinations at cryogenic conditions with the synthetic technique. The experimental setup consists of a visual equilibrium cell that includes a transparent sapphire tube and two stainless steel (SAE316L) flanges, as shown in Fig. 2. The cell has an internal volume of 75 mL and a pressure rating of 31 MPa. A Digiquartz Paroscientific pressure transducer with a full scale of 41 MPa and relative standard uncertainty of 0.01 % of the full scale is used to measure the system's pressure. A magnetic stirrer, driven by a stepper motor (Arun Microelectronics), is placed inside the cell to ensure mixture homogeneity during phase equilibrium measurements.

A cryogenic environmental chamber (M170J-13100) with an operating temperature range of (87 to 473) K housed the visual cell and controlled bulk fluid temperature (Thermal Solution Series—KTS6310AB). To minimise thermal shock risk for the sapphire tube, the cooling and heating rates of the chamber were controlled to a maximum of 1 K·min⁻¹ by adjusting the liquid nitrogen flow from a high-pressure Dewar. Three fast-response 100 Ω platinum resistance thermometers (PRT NR-14, Netsushin) were employed to measure the cell temperature and were placed into holes bored on the top and bottom flanges and the copper tip inside the cell. The PRTs were calibrated against a reference standard temperature sensor (ASL-WIKA) with 0.02 K standard uncertainty over temperatures between (100 and 273) K. The mean temperature difference between these PRTs at the top and bottom of the cell was less than 0.1 K during the equilibrium condition. For the SFE measurements, the copper tip temperature was taken as the measure of the observed freezing and melting points. A Panasonic high-definition (HD) camcorder (HCV 180) captured and recorded observations of solid freezing and melting.

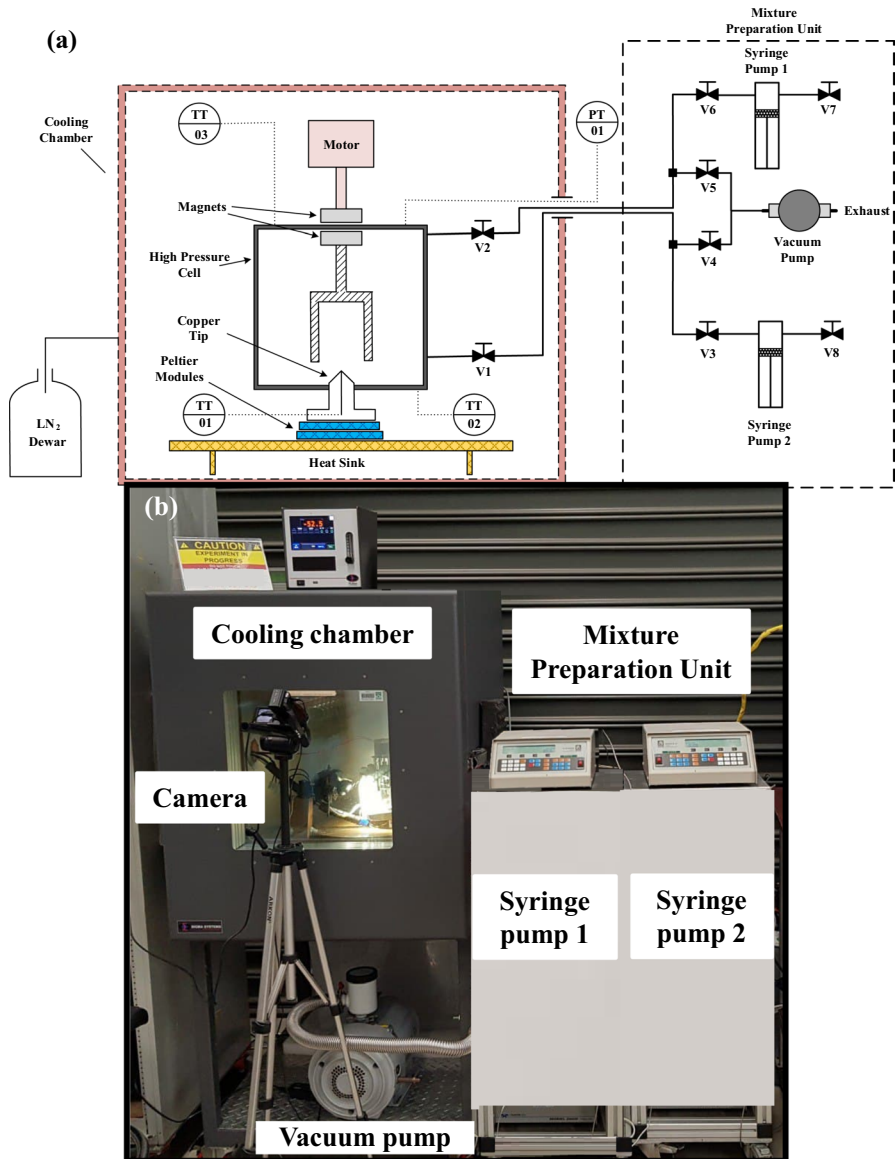
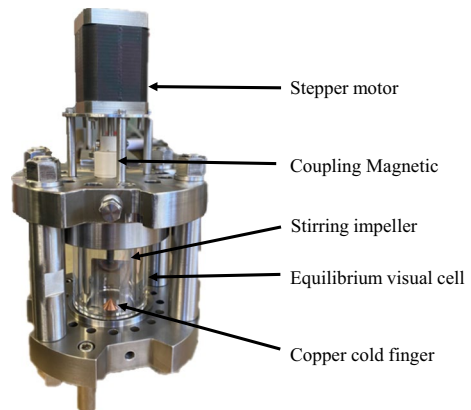


Fig. 1 (a) Schematic diagram of the SFE apparatus; (b) photograph of the measurement setup

3 Mixture Preparation for SFE Measurements

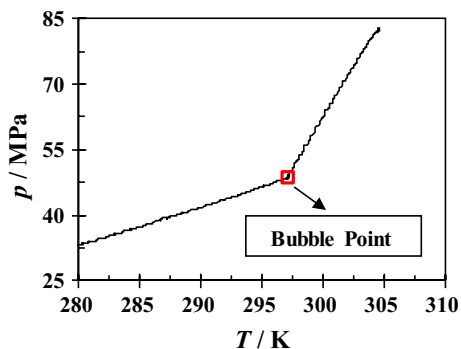
Before preparing a mixture for the SFE measurements, the visual cell and all connections were cleaned and evacuated using the vacuum pump (Varian SH-110). The HFC-32 + CO₂ binary mixtures were prepared in two different approaches. For binary mixtures of (80 to 95) mol % CO₂, a predetermined volume of pure HFC-32

Fig. 2 Photograph of the equilibrium cell



was injected into the cell, and the mixture composition was then adjusted by injecting CO_2 in increments of 5 mol %. Additionally, the mixtures with CO_2 compositions of (11, 28, 51 and 72) mol % were prepared by injecting the predetermined amounts of HFC-32 and CO_2 into a high-precision syringe pump. The prepared mixtures were pressurised at (8 and 11) MPa, higher than the mixture's cricondenbar pressure calculated using the Helmholtz energy models implemented in REFPROP 10 [5, 28], to ensure the samples were in a single-phase condition during the storage and transfer to the cell. The bottom section of the syringe pump's cylinder was also heated at 328 K to ensure the mixture's homogeneity by allowing convective mixing inside the syringe pump. The cell was connected to the syringe pump and the single-phase mixture was injected into the cell while the syringe pump remained pressurised at 8 MPa at all times. Once the pressure in the equilibrium cell had reached 8 MPa, it was left to stabilise at constant pressure for 6 h while being repeatedly stirred on an intermittent basis (20 s stirring at 300 rpm, 20 s of no stirring) to ensure the sample in the cell was a well-mixed and homogenous single-phase mixture. At this high pressure, samples taken using the ROLSI valves would saturate the GC column, meaning that the analytical method could not be used to verify the overall mixture composition. Instead, the bubble point of the sample was measured and compared with the prediction of the previously optimised Helmholtz EOS [13] for this mixture to confirm that it was well-mixed and the sample composition was close to the volumetrically determined value. The sample was then pressurised at room temperature to between (8 and 11) MPa (well above the mixture's cricondenbar pressure), to ensure its density would be sufficient to reach a bubble point upon isochoric cooling (based on Helmholtz EOS [13] calculations of the fluid mixture's density). To measure the sample's bubble point via the synthetic method, the cell was isolated, and the sample was cooled at a controlled rate of $0.8 \text{ K} \cdot \text{min}^{-1}$ as shown in Fig. 3. The cooling rate of $0.8 \text{ K} \cdot \text{min}^{-1}$ was sufficiently slow to mitigate thermal lags and produce bubble-points consistent with those expected based on the overall mixture composition and the isochor's density, within the combined uncertainty in the overall composition of the synthetic binary mixtures (0.01 CO_2 mole fraction).

Fig. 3 The pressure–temperature (PT) diagram during the isochoric cooling of the HFC-32 + CO₂ (28:72 mol %) binary mixture to synthetically determine the bubble point. The red square corresponds to the predicted bubble point (Color figure online)



3.1 Melting and Freezing Measurement Procedures

After loading the cell, the cooling chamber temperature was reduced at a rate of 0.8 K·min⁻¹ until stabilised by control algorithms at the desired set-points. Then, the temperature was gradually reduced at a rate between (0.1 and 0.25) K·min⁻¹ until solid crystals were formed. The observed temperature and pressure of this point were recorded as the freezing point (T_f and p_f) of the sample. After forming the solids in the cell, the temperature was increased in steps of (0.1 to 1) K every 20 min (corresponding to an average heating rate between (0.005 and 0.05) K·min⁻¹) until complete melting was observed. The temperature and pressure of this point were recorded as the melting point (T_m and p_m) of the sample. Each melting point measurement was repeated three times.

3.2 Uncertainty Analysis

The uncertainty analysis for the SFE measurements was conducted based on the "Guide to the Expression of Uncertainty in Measurement (GUM)" method [29]. In this study, standard uncertainties with a coverage factor of $k=1$ are reported. The standard uncertainties in the measured melting temperatures were estimated to be the standard deviation of the repeated measurements for each point (0.3 K), which is significantly larger than the intrinsic and calibration uncertainties of the PRT sensors (0.05 K). This uncertainty analysis carried out by Siahvashi et al. [19, 20] revealed that temperature fluctuations were the dominant contribution to the experimental uncertainty. Similarly, repeated freezing temperature measurements at each point had a standard deviation of 0.3 K. The estimated standard uncertainty in pressure measurements was 0.02 MPa, which reflected the pressure fluctuations resulting from the thermal stability of the apparatus (the intrinsic and calibration uncertainties for the pressure sensor were negligible).

The standard uncertainty in the overall composition of the synthetic binary mixtures was mainly affected by the uncertainties in the injected volumes from the syringe pumps and the pure fluid densities under the syringe pumps' conditions. The relative standard uncertainties in the densities of the pure samples in the syringe

pumps' conditions (pressures up to 11 MPa at room temperature) were estimated to be around 1 % considering the temperature and pressure measurement uncertainties for the syringe pumps; the uncertainty contributions of the Helmholtz EOS implemented in REFPROP 10 [5, 28, 30] were negligible. The overall relative standard uncertainty associated with the syringe pumps' injected volumes was 0.3 % [19]. The average combined uncertainty in the overall composition of the synthetic binary mixtures used for the SFE measurements was 0.01 CO₂ mole fraction.

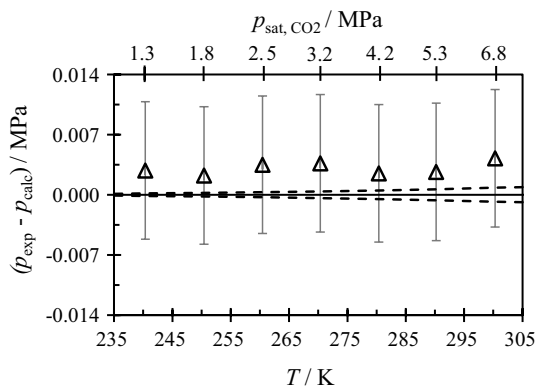
3.3 Apparatus Validation

The Paroscientific pressure sensor's readings for the pure N₂ gas at pressures between (0.1 and 23) MPa were validated against the values measured by a reference pressure transmitter (Mensor/Wika CPT9000). The Mensor CPT9000 pressure transmitter was calibrated and certified by the accredited Australian Pressure Laboratory over a pressure range of (0.1 and 41) MPa with a standard uncertainty of 0.004 MPa. The difference in the reading of the two pressure sensors for the investigated pressure range was within the standard uncertainties of the sensors.

Further validations of the apparatus involved comparing the measured vapour pressure of pure CO₂ at a temperature range of (240 to 300) K with those predicted by the CO₂ reference EOS developed by Span and Wagner [5]. Figure 4 shows the deviations between the measured pressure (p_{exp}) and the predicted pressure (p_{calc}) by the EOS while the measured temperatures were the input to the EOS. The deviations did not exceed the standard uncertainty of the experimental data.

To validate the visual melting point measurement method, the triple point of the pure CO₂ was measured to be 216.6 K at 0.53 MPa, which is in good agreement with the reference triple point temperature of 216.55 K at 0.518 MPa reported by Span and Wagner [5]. Additionally, the triple point temperature of pure HFC-32 was measured to be 135.3 K, around 1 K lower than the reported triple point temperatures by Di Nicola et al. [31] and Lüddecke and Magee [32]. Those studies used a visual evaluation of the experimental P–T profile for the fluid to locate the triple point of HFC-32 by noting a sharp break in the temperature rise rate, assuming the solid melting process was started. However, in this study, the triple points of the

Fig. 4 Deviations $\Delta p = (p_{\text{exp}} - p_{\text{calc}})$ between the experimental vapour pressure of pure CO₂ (p_{exp}) and values (p_{calc}) from the reference Helmholtz EOS [5] as a function of the observed temperature (T): (Δ , black), this work. The error bars show the standard uncertainty of the experimental data, and the dashed lines represent the uncertainty of the calculated CO₂ vapour pressures as specified by Span and Wagner [5]



pure CO₂ and HFC-32 were measured visually and correspond to when complete melting was observed, as shown in Fig. 5.

4 Thermodynamic Modelling

In this work, the measured SFE data are compared with predictions of thermodynamic model embedded in ThermoFAST software package [24]. At SFE, the fugacity of the CO₂ fraction in the fluid mixture is equal to the fugacity of CO₂ in the solid phase:

$$f_{\text{CO}_2}^{\text{S}}(p, T) = f_{\text{CO}_2}^{\text{fluid}}(p, T, z_{\text{CO}_2}), \quad (1)$$

where z_{CO_2} is the CO₂ mole fraction in the fluid mixture. The fugacity of pure solid CO₂ may be calculated using the reference Helmholtz EOS for solid phase (I) CO₂ developed by Trusler [23] as follows:

$$\ln\left(\frac{f_{\text{CO}_2}^{\text{S}}}{p}\right) = \frac{A^r}{RT} - \frac{1}{RTV} \left(\frac{\partial A^r}{\partial V}\right)_T - \ln\left[1 - \frac{1}{RTV} \left(\frac{\partial A^r}{\partial V}\right)_T\right] \quad (2)$$

where R is the universal gas constant, V is the volume, and p and T are the experimental pressures and temperatures, respectively. The term A^r represents the residual Helmholtz energy at the experimental condition, calculated by the difference between the Helmholtz energy, $A(T, p)$, and the ideal-gas Helmholtz energy, $A^0(T)$, where no intermolecular forces exist.

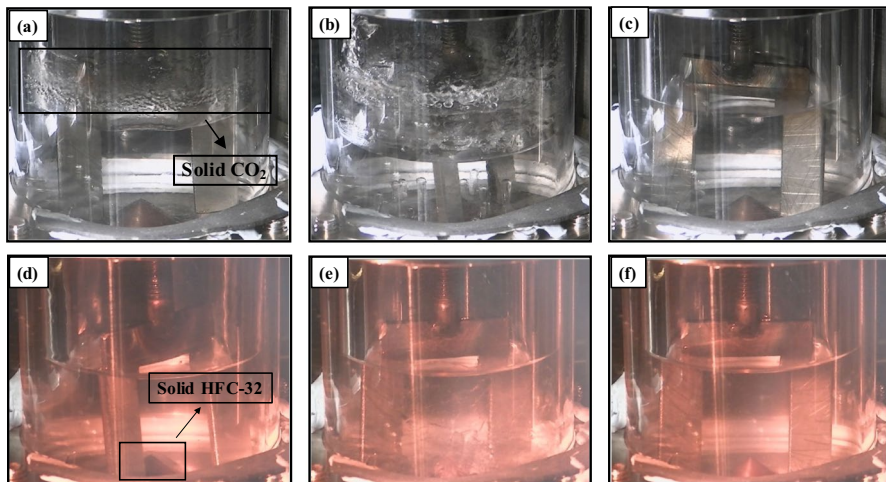


Fig. 5 The triple point measurement procedure for pure CO₂ (a–c) and HFC-32 (d–f): (a) freezing point of CO₂ ($p=0.518$ MPa, $T=215.7$ K), (b) $p=0.48$ MPa, $T=215.6$ K, and (c) melting point of CO₂ ($p=0.526$ MPa, $T=216.6$ K). (d) Freezing point of HFC-32 ($p=0.02$ MPa, $T=134.4$ K), (e) $p=0.02$ MPa, $T=134$ K, (f) melting point of HFC-32 ($p=0.02$ MPa, $T=135.3$ K)

The 1976 Peng–Robinson equation of state (PR-EOS) was used to calculate the term $f_{\text{CO}_2}^{\text{fluid}}$. This cubic EOS was chosen because it can be easily tuned to predict phase equilibrium for mixtures, particularly when limited experimental data are available, and it is computationally simple. The PR-EOS is described as follows [22]:

$$p = \frac{RT}{v - b} - \frac{a}{v^2 + 2bv - b^2} \quad (3)$$

Here, v is the molar volume and parameters a and b represent the temperature-dependent energy and co-volume parameters, respectively. The van der Waals one-fluid mixing rules that incorporate a single temperature-independent BIP (k_{ij}) can be used to correlate the mixtures' thermodynamic properties.

$$a = \sum_i \sum_j x_i x_j (1 - k_{ij}) \sqrt{a_i a_j} \quad (4)$$

$$b = \sum_i x_i b_i \quad (5)$$

These models are implemented in ThermoFAST with a default BIP (k_{ij}) of zero for the SFE calculations of the HFC-32 + CO₂ binary system. This BIP was subsequently adjusted by regression to the experimental melting data measured in this work. This regression to the melting data means that calculations of other properties such as VLE should be considered less accurate; as discussed by Baker et al. [33], it is for this reason that the ThermoFAST uses a different set of BIPs for VLE-only calculations. The best-fit value of the SFE BIP for CO₂-HFC-32 was determined by minimising the root mean square deviation (RMSD) of the experimental (T_{exp}) and calculated (T_{calc}) melting temperatures as follows:

$$\text{RMSD}_T = \sqrt{\frac{\sum_{i=1}^N [T_{\text{exp},i} - T_{\text{calc},i}]^2}{N}} \quad (6)$$

Here, N is the total number of the points used in optimising the BIP and i stands for an individual data point.

In principle, the multi-fluid Helmholtz energy EOS for HFC-32 + CO₂ binary reported by Xiao et al. [14] could also be used to predict the SFE. However, tuning multi-fluid mixture models requires significant quantities of data, ideally for multiple thermodynamic properties, otherwise their accuracy can become significantly compromised. Furthermore, selecting which of the model's four BIPs to adjust to tune it to better represent the SFE is not straightforward. For these reasons, we chose not to tune the multi-fluid Helmholtz EOS to the SFE data and focussed on developing a targeted model optimised only for predicting melting temperatures in mixtures. We recommend that for other thermodynamic properties of the HFC-32 + CO₂ binary, the model reported by Xiao et al. [14] be used.

5 Results and Discussion

5.1 SFE Measurement Data

The melting and freezing temperatures of the HFC-32 + CO₂ binary system were measured for mixtures with CO₂ compositions between (0 and 100) mol %. Table 2 presents the average freezing and melting temperatures and pressures at different overall compositions of the binary mixtures measured in this study.

Near the SLVE line, the freezing and melting temperatures were measured isochorically at the vapour pressure of the mixture, while near at the SLE condition, the measurements were carried out isobarically at pressures of (8 and 11) MPa. Figure 6a–c show the freezing and melting measurements for the HFC-32 + CO₂ (72:28 mol %) mixture at SLVE, and Fig. 6d–f shows the measurements at 8 MPa when the mixture was at SLE. The HFC-32 + CO₂ binary systems generally needed an average sub-cooling of 1.7 K to initiate solid formation.

Figure 7 shows the melting temperature of solids in the HFC-32 + CO₂ binary system against the different CO₂ compositions measured in this work, together with the reported data by Di Nicola et al. [7]. The melting temperature of CO₂

Table 2 Measured SFE data for the HFC-32 + CO₂ binary mixtures at different CO₂ mole fractions and operating pressures

Phase	$X_{\text{HFC-32}}$	x_{CO_2}	T_f/K	p_f/MPa	T_m/K	p_m/MPa
SLVE	0.00	1.00	216.0	0.52	216.6	0.53
SLVE	0.05	0.95	214.2	0.46	214.9	0.47
SLVE	0.10	0.90	212.1	0.42	212.6	0.41
SLVE	0.15	0.85	209.2	0.35	210.2	0.36
SLVE	0.20	0.80	207.1	0.30	208.0	0.31
SLVE	0.28	0.72	201.3	0.20	201.9	0.21
SLE	0.28	0.72	203.0	8.09	203.7	8.09
SLE	0.28	0.72	204.2	11.08	204.5	11.08
SLVE	0.49	0.51	186.2	0.06	187.5	0.07
SLE	0.49	0.51	187.7	8.08	189.2	8.09
SLE	0.49	0.51	186.7	11.07	189.7	11.07
SLVE	0.72	0.28	162.4	0.02 ^a	165.5	0.02 ^a
SLE	0.72	0.28	161.3	8.06	166.3	8.07
SLE	0.72	0.28	165.9	10.99	167.1	11.05
SLVE	0.89	0.11	128.9	0.02 ^a	131.9	0.02 ^a
SLE	0.89	0.11	129.9	8.06	132.7	8.09
SLE	0.89	0.11	130.9	11.06	133.0	11.07
SLVE	1.00	0.00	134.4	0.02 ^a	135.3	0.02 ^a

The standard uncertainties in temperature, $u(T)$, pressure, $u(p)$, and CO₂ mole fractions, $u(z_{\text{CO}_2})$, are 0.3 K, 0.02 MPa, and 0.01, respectively

^aThe resolution limit of the pressure measurement is 0.02 MPa when performing cooling/heating ramps. The actual pressure is likely to be close to the vapour pressure of HFC-32

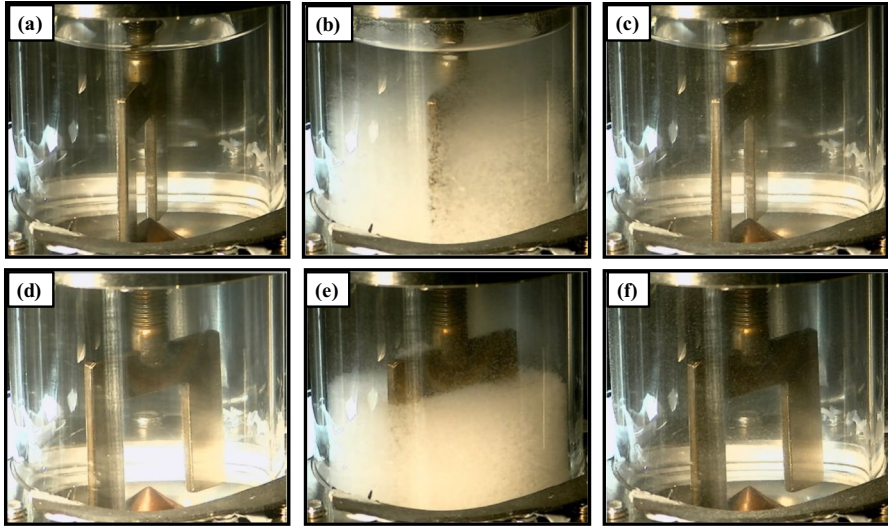
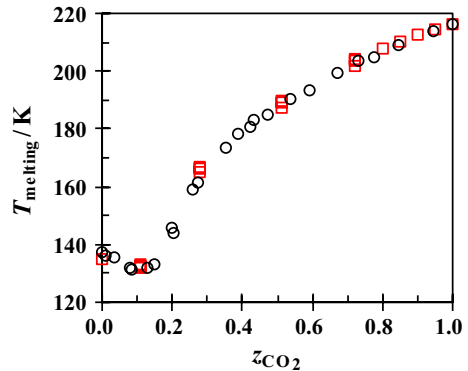


Fig. 6 The freezing and melting points measurement for the HFC-32+CO₂ (72:28 mol %) at the SLVE (a)–(c) and SLE (d)–(f) conditions: (a) sub-cooled VLE ($p=0.02$ MPa, $T=162.4$ K); (b) freezing point—SLVE ($p=0.02$ MPa, $T=162.4$ K); and (c) melting point—SLVE ($p=0.02$ MPa, $T=165.5$ K); (d) sub-cooled liquid ($p=8.1$ MPa, $T=161.3$ K); (e) freezing point—SLE ($p=8.1$ MPa, $T=161.3$ K); and (f) melting point—SLE ($p=8.1$ MPa, $T=166.3$ K)

Fig. 7 The temperature-composition ($T-z_{\text{CO}_2}$) diagram for the experimental melting points of the CO₂ in the HFC-32 + CO₂ binary system: this work (\square); Di Nicola et al. [7] (\circ)



decreased from (216.6 to 165.5) K with the addition of 72 mol % HFC-32 to the pure CO₂ sample. Increasing the fraction of HFC-32 to 89 mol % resulted in complete freezing of the fluid phase at temperatures below 129 K, with complete melting of the solids achieved at 131.9 K under SLVE. This melting temperature is lower than the melting temperatures of both pure HFC-32 (135.3 K) and CO₂ (216.6 K), showing the presence of a eutectic [7].

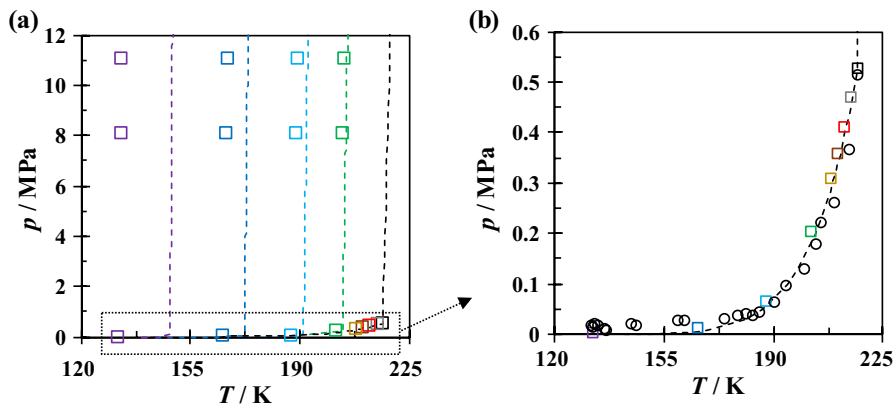


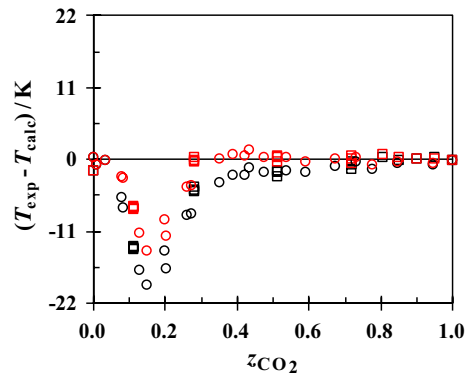
Fig. 8 (a) The P–T data for the melting points of the HFC-32 + CO₂ binary system. The insert (b) shows the SLVE data, together with the reported data by Di Nicola et al. [7]: this work (□), Di Nicola et al. [7] (○) --- melting temperature predicted by ThermoFAST using the default BIP of zero; compositions: black (100 mol % CO₂), grey (95 mol % CO₂), red (90 mol % CO₂), brown (85 mol % CO₂), yellow (80 mol % CO₂), green (72 mol % CO₂), light-blue (51 mol % CO₂), dark-blue (28 mol % CO₂), and purple (11 mol % CO₂) (Color figure online)

5.2 Model Tuning

Figure 8a shows the measured melting points for the HFC-32 + CO₂ binary system, together with the predictions of the default ThermoFAST model. The melting data measured at SLVE (Fig. 8b) follow the pure CO₂ sublimation curve. Using the default BIP of zero in the PR-EOS for the HFC-32 + CO₂ binary system, the untuned ThermoFAST model represented the measured melting points with an RMSD of 7.3 K. Additionally, a multi-fluid Helmholtz energy EOS [13] (with its default BIPs) was used for the fluid phase calculations in ThermoFAST along with the Helmholtz EOS for the CO₂ solid phase [23], resulting in an RMSD of 9.1 K from the measured melting data. The smaller deviation observed when the untuned PR-EOS was used for the fluid phase calculations possibly reflects its robust phase equilibrium predictions for mixtures and relatively simple functional form, while the Helmholtz model has been tuned to represent many single-phase properties of the fluid mixture measured at higher temperatures. Its more complex functional form means that extrapolating the Helmholtz model is likely to produce less accurate estimates of properties particularly for those not used in its development. In this study, the ThermoFAST model with PR-EOS for the fluid phase was tuned to the SFE (melting temperatures only) data measured in this work, with the understanding that such tuning would likely make the resulting PR EOS less accurate for the prediction of other fluid mixture properties.

Tuning the model to the measured melting data by adjusting the BIP decreased the RMSD by 60 %, from (7.3 to 3) K, with an optimised BIP of ($k_{ij} = -0.024$). Figure 9 shows the differences between the experimental melting points and predicted values by the default and tuned ThermoFAST models. In this plot, the abscissa is the CO₂ mole fraction in the HFC-32 + CO₂ mixture and the ordinate is the difference

Fig. 9 Absolute difference between the measured melting temperature (T_{exp}) and correlated values (T_{calc}) by the default (black) and tuned (red) ThermoFAST models for the HFC-32 + CO₂ binary system: this work (□), Di Nicola et al. [7] (○) (Color figure online)



between the measured and calculated equilibrium melting temperatures. The RMSD of the model calculations from the melting point data reported by Di Nicola et al. [7] improved by 46 %, from (9.1 to 4.9) K, by this optimisation. For mixtures with a CO₂ fraction over 0.28, the tuned model represents the melting point data with an RMSD of 0.5 K, which is 87 % lower than the default model. For the eutectic composition (11 mol% CO₂), the tuned model predicts a mixture melting temperature 7.6 K higher than the measured values against the default model's deviation of 16.3 K and the Helmholtz energy EOS' [13] deviation of 20.1 K. A better representation of eutectic composition would likely be achieved if the solid phase model included correlations for the HFC-32 solid phase fugacity.

6 Conclusions

New SFE data for the HFC-32 + CO₂ binary system were measured at CO₂ fractions between (0 and 100) mol%. The experimental data reported in this study and the literature data show a eutectic composition of around 11 mol% CO₂ with a eutectic temperature of 131.9 K at an SLVE condition. The measured melting data were compared with the predictions of a thermodynamic model constructed by combining the Peng–Robinson 1976 EOS with van der Waals one-fluid mixing rules for the fluid phase and a reference Helmholtz EOS for the CO₂ solid phase. The binary interaction parameter of the model was then adjusted by regression to the measured melting data. The tuned model could represent the melting data with an RMSD of 3.2 K, 60% better than the default model. The RMSD for the mixtures with the CO₂ fractions over 28 mol% was 0.5 K for the tuned model against an RMSD of 3.4 K for the default model. This work provides new SFE data for the HFC-32 + CO₂ binary system that are useful to the design refrigeration systems utilising eco-friendly refrigerant mixtures with up to 80% less GWP than currently-used working fluids.

Author Contributions Conceptualization: EM, PS, AA; methodology: MS, AS, SA; formal analysis and investigation: MS, AS, SA, PS, EM; writing—original draft preparation: MS; Writing—review and editing: AA, TT, AY, YY, PS, EM; funding acquisition: EM, PS; supervision: PS, EM.

Funding Open Access funding enabled and organized by CAUL and its Member Institutions. This study was funded by Mitsubishi Heavy Industries, Ltd.

Data Availability All experimental data are presented in Sect. 4, Table 2.

Declarations

Competing interests The authors have no competing interests to declare that are relevant to the content of this article.

Ethical Approval The work contains no libelous or unlawful statements, does not infringe on the rights of others, or contains material or instructions that might cause harm or injury.

Open Access This article is licensed under a Creative Commons Attribution 4.0 International License, which permits use, sharing, adaptation, distribution and reproduction in any medium or format, as long as you give appropriate credit to the original author(s) and the source, provide a link to the Creative Commons licence, and indicate if changes were made. The images or other third party material in this article are included in the article's Creative Commons licence, unless indicated otherwise in a credit line to the material. If material is not included in the article's Creative Commons licence and your intended use is not permitted by statutory regulation or exceeds the permitted use, you will need to obtain permission directly from the copyright holder. To view a copy of this licence, visit <http://creativecommons.org/licenses/by/4.0/>.

References

1. D. Shindell, F. Bréon, W. Collins, J. Fuglestedt, J. Huang, D. Koch et al., Anthropogenic and Natural Radiative Forcing, in *Climate Change 2013: The Physical Science Basis. Contribution of Working Group I to the Fifth Assessment Report of the Intergovernmental Panel on Climate Change* (2013)
2. M.S. Sadaghiani, A. Arami-Niya, D. Zhang, T. Tsuji, Y. Tanaka, Y. Seiki et al., Minimum ignition energies and laminar burning velocities of ammonia, HFO-1234yf, HFC-32 and their mixtures with carbon dioxide, HFC-125 and HFC-134a. *J. Hazard. Mater.* **407**, 124781 (2021)
3. Y. Chernyak, P. Zhelezny, M. Paulaitis, Thermodynamic properties of HFC-32 / HFC-125 mixtures and an estimation of its environmental impact and utility in refrigeration, in *International Refrigeration and Air Conditioning Conference*, p. 360 (1996). <http://docs.lib.purdue.edu/iracc/360>
4. UNEP, The Kigali Amendment to the Montreal Protocol: HFC Phase-down, in *28th Meeting of the Parties to the Montreal Protocol*, 10–14 October 2016, Kigali, Rwanda, pp. 1–7 (2016)
5. R. Span, W. Wagner, A new equation of state for carbon dioxide covering the fluid region from the triple-point temperature to 1100 K at pressures up to 800 MPa. *J. Phys. Chem. Ref. Data* **25**, 1509–1596 (1996). <https://doi.org/10.1063/1.555991>
6. C. Meyers, M. Van Dusen, The vapor pressure of liquid and solid carbon dioxide. *Bureau Stand. J Res* **10**, 381–412 (1933)
7. G. Di Nicola, G. Giuliani, F. Polonara, R. Stryjek, Soli-liquid equilibria for the CO₂ + N₂O, CO₂ + R₃₂, and N₂O + R₃₂ systems. *Fluid Phase Equilib.* **256**, 86–92 (2007). <https://doi.org/10.1016/j.fluid.2006.11.015>
8. G. Di Nicola, F. Polonara, R. Stryjek, Burnett measurements for the difluoromethane + carbon dioxide system. *J. Chem. Eng. Data* **47**, 876–881 (2002). <https://doi.org/10.1021/je015537m>
9. N.G. Di, M. Pacetti, F. Polonara, R. Stryjek, Isochoric Measurements for CO₂ + R₁₂₅ and CO₂ + R₃₂ Binary Systems. *J. Chem. Eng. Data* **47**, 1145–1153 (2002). <https://doi.org/10.1021/je015541y>
10. A. Diefenbacher, M. Türk, (Vapour + liquid) equilibria of binary mixtures of CO₂, CH₂F₂, CHF₃, and SF₆. *J. Chem. Thermodyn.* **34**, 1361–1375 (2002). [https://doi.org/10.1016/S0021-9614\(02\)00123-4](https://doi.org/10.1016/S0021-9614(02)00123-4)
11. R.A. Adams, F.P. Stein, Vapor-liquid equilibria for carbon dioxide-difluoromethane system. *J. Chem. Eng. Data* **16**, 146–149 (1971). <https://doi.org/10.1021/je60049a015>
12. F. Rivollet, A. Chapoy, C. Coquelet, D. Richon, Vapor-liquid equilibrium data for the carbon dioxide (CO₂) + difluoromethane (R₃₂) system at temperatures from 283.12 to 343.25 K and pressures up to 7.46 MPa. *Fluid Phase Equilib.* **218**, 95–101 (2004). <https://doi.org/10.1016/j.fluid.2003.12.002>

13. A. Arami-Niya, X. Xiao, S.Z.S. Al Ghafri, F. Jiao, M. Khamphasith, E. Sadeghi Pouya et al., Measurement and modelling of the thermodynamic properties of carbon dioxide mixtures with HFO-1234yf, HFC-125, HFC-134a, and HFC-32: vapour–liquid equilibrium, density, and heat capacity. *Int. J. Refrig* **118**, 514–528 (2020). <https://doi.org/10.1016/j.iijrefrig.2020.05.009>
14. X. Xiao, L. Tenardi, M. Seyyedsadaghiani, E.S. Pouya, X. Yang, S.A. Ghafri et al., Thermodynamic property measurements and modelling of CO₂ + difluoromethane (R₃₂): density, heat capacity, and vapour–liquid equilibrium: Mesures et modélisation des propriétés thermodynamiques du CO₂ + difluorométhane (R₃₂): masse volumique, capacité calorifique et équilibre vapeur-liquide. *Int. J. Refrig.* (2022). <https://doi.org/10.1016/j.iijrefrig.2022.11.029>
15. J. Gernert, R. Span, EOS–CG: a Helmholtz energy mixture model for humid gases and CCS mixtures. *J Chem Thermodyn* **93**, 274–293 (2016). <https://doi.org/10.1016/J.JCT.2015.05.015>
16. A. Jäger, R. Span, Equation of state for solid carbon dioxide based on the Gibbs free energy. *J. Chem. Eng. Data* **57**, 590–597 (2012). <https://doi.org/10.1021/je2011677>
17. J. Gernert, A. Jäger, R. Span, Calculation of phase equilibria for multi-component mixtures using highly accurate Helmholtz energy equations of state. *Fluid Phase Equilib.* **375**, 209–218 (2014). <https://doi.org/10.1016/j.fluid.2014.05.012>
18. S. Hielscher, B. Semrau, A. Jäger, V. Vinš, C. Breitkopf, J. Hrubý et al., Modification of a model for mixed hydrates to represent double cage occupancy. *Fluid Phase Equilib.* **490**, 48–60 (2019). <https://doi.org/10.1016/j.fluid.2019.02.019>
19. A. Siahvashi, S.Z.S. Al Ghafri, E.F. May, Solid–fluid equilibrium measurements of benzene in methane and implications for freeze-out at LNG conditions. *Fluid Phase Equilib.* **519**, 112609 (2020). <https://doi.org/10.1016/j.fluid.2020.112609>
20. A. Siahvashi, S.Z.S. Al Ghafri, X. Yang, D. Rowland, E.F. May, Avoiding costly LNG plant freeze-out-induced shutdowns: measurement and modelling for neopentane solubility at LNG conditions. *Energy* **217**, 119331 (2021). <https://doi.org/10.1016/j.energy.2020.119331>
21. M.S. Sadaghiani, A. Siahvashi, B.W.E. Norris, S.Z.S. Al Ghafri, A. Arami-Niya, E.F. May, Prediction of solid formation conditions in mixed refrigerants with iso-pentane and methane at high pressures and cryogenic temperatures. *Energy* **250**, 123789 (2022). <https://doi.org/10.1016/j.energy.2022.123789>
22. D.-Y. Peng, D.B. Robinson, A new two-constant equation of state. *Ind. Eng. Chem. Fundam.* **15**, 59–64 (1976). <https://doi.org/10.1021/i160057a011>
23. J.P. Martin Trusler, Equation of state for solid phase I of carbon dioxide valid for temperatures up to 800 K and pressures up to 12 GPa. *J. Phys. Chem. Ref. Data* (2011). <https://doi.org/10.1063/1.3664915>
24. P.E. Falloon, C.J. Baker, D. Rowland, V. Jusko, D. Zhu, X. Xiao et al. ThermoFAST 2. Thermodynamic calculator for natural gas properties. *Fluid Science and Resources*, The University of Western Australia, Crawley (2022)
25. A. Siahvashi, S.Z.S. Al-Ghafri, J.H. Oakley, T.J. Hughes, B.F. Graham, E.F. May, Visual measurements of solid–liquid equilibria and induction times for cyclohexane + octadecane mixtures at pressures to 5 MPa. *J. Chem. Eng. Data* **62**, 2896–2910 (2017). <https://doi.org/10.1021/acs.jced.7b00171>
26. A. Siahvashi, Visual measurements of solid–fluid equilibria in hydrocarbon mixtures for enhanced LNG production. Doctoral Thesis, The University of Western Australia (2019)
27. A. Siahvashi, S.Z.S. Al Ghafri, T.J. Hughes, B.F. Graham, S.H. Huang, E.F. May, Solubility of p-xylene in methane and ethane and implications for freeze-out at LNG conditions. *Exp. Therm. Fluid Sci.* **105**, 47–57 (2019). <https://doi.org/10.1016/J.EXPTHERMFLUSCI.2019.03.010>
28. R. Tillner-Roth, A. Yokozeki, An international standard equation of state for difluoromethane (R-32) for temperatures from the triple point at 136.34 K to 435 K and pressures up to 70 MPa. *J. Phys. Chem. Ref. Data* **26**, 1273–328 (1997). <https://doi.org/10.1063/1.556002>
29. JCGM, Evaluation of measurement data—guide to the expression of uncertainty in measurement (JCGM 100:2008), BIPM (2008)
30. E.W. Lemmon, I.H. Bell, M.L. Huber, M.O. McLinden, NIST Standard Reference Database 23: Reference Fluid Thermodynamic and Transport Properties-REFPROP, Version 10.0, National Institute of Standards and Technology, p. 135 (2018). <https://doi.org/10.18434/T4/1502528>
31. N.G. Di, C. Brandoni, N.C. Di, G. Giuliani, Triple point measurements for alternative refrigerants. *J. Therm. Anal. Calorim.* **108**, 627–631 (2012). <https://doi.org/10.1007/s10973-011-1944-4>
32. T.O. Lüddecke, J.W. Magee, Molar heat capacity at constant volume of difluoromethane (R32) and pentafluoroethane (R125) from the triple-point temperature to 345 K at pressures to 35 MPa. *Int. J. Thermophys.* **17**, 823–849 (1996). <https://doi.org/10.1007/bf01439192>

33. C. Baker, A. Siahvashi, J. Oakley, T. Hughes, D. Rowland, S. Huang et al., Advanced predictions of solidification in cryogenic natural gas and LNG processing. *J. Chem. Thermodyn.* **137**, 22–33 (2019). <https://doi.org/10.1016/j.jct.2019.05.006>

Publisher's Note Springer Nature remains neutral with regard to jurisdictional claims in published maps and institutional affiliations.

Authors and Affiliations

Mirhadi S. Sadaghiani¹ · Arman Siahvashi¹ · Arash Arami-Niya^{1,2} · Tomoya Tsuji³ · Atsuhiko Yukumoto⁴ · Yoshio Seiki⁴ · Saif Z. S. Al Ghafri¹ · Paul L. Stanwix¹ · Eric F. May^{1,5}

✉ Eric F. May
Eric.May@uwa.edu.au

- ¹ Fluid Science & Resources Division, Department of Chemical Engineering, The University of Western Australia, 35 Stirling Hwy, Crawley 6009, Australia
- ² Discipline of Chemical Engineering, Western Australian School of Mines: Minerals, Energy and Chemical Engineering, Curtin University, GPO Box U1987, Perth, WA 6845, Australia
- ³ Malaysia-Japan International Institute of Technology, Universiti Teknologi Malaysia, 54100 Kuala Lumpur, Malaysia
- ⁴ Chemical No. 2 Laboratory, Chemical Research Department, Research & Innovation Center, Mitsubishi Heavy Industries, Ltd, 717-1, Fukahori-Machi, 5-Chome, Nagasaki 851 0392, Japan
- ⁵ Future Energy Exports Cooperative Research Centre, 35 Stirling Hwy, Crawley, WA 6009, Australia